

## Experimental Work Conducted on MgO Characterization and Hydration

Haoran Deng<sup>1</sup>, Yongliang Xiong<sup>1</sup>, Martin Nemer<sup>2</sup> and Shelly Johnsen<sup>1</sup>

<sup>1</sup>Repository Performance Dept. 6712

<sup>2</sup>Performance Assessment and Decision Analysis Dept. 6711

Sandia National Laboratories Carlsbad Programs Group, Carlsbad, NM 88220

### ABSTRACT

Magnesium oxide (MgO) is the only engineered barrier certified by the EPA for emplacement in the Waste Isolation Pilot Plant (WIPP), a U.S. Department of Energy repository for transuranic waste. MgO will reduce actinide solubilities by sequestering CO<sub>2</sub> generated by the biodegradation of cellulosic, plastic, and rubber materials. Demonstration of the effectiveness of MgO is essential to meet the U.S Environmental Protection Agency's requirement for multiple natural and engineered barriers. In the past, a series of experiments was conducted at Sandia National Laboratories to verify the efficacy of Premier Chemicals LLC (Premier) MgO as a chemical-control agent in the WIPP. Since December 2004, Premier MgO is no longer available for emplacement in the WIPP. Martin Marietta Magnesia Specialties LLC is the new MgO supplier. MgO characterization, including chemical, mineralogic, and reactivity analysis, has been performed to address uncertainties concerning the amount of reactive constituents in Martin Marietta MgO. Characterization results of Premier MgO will be reported for comparison.

Particle size, solid-to-liquid ratio, and stir speed could affect the rate of carbonation of MgO slurries. Thus, it's reasonable to hypothesize that these factors will also affect the rate of hydration. Accelerated MgO hydration experiments were carried out at two or three levels for each of the above factors in deionized water at 70 °C. The Minitab statistical software package was used to design a fractional-factorial experimental matrix and analyze the test results. We also fitted the accelerated inundated hydration data to four different kinetic models and calculated the hydration rates. As a result of this study we have determined that different mechanisms may be important for different particle sizes, surface control for large particles and diffusion for small particles.

### INTRODUCTION

The Waste Isolation Pilot Plant (WIPP) is a U.S. Department of Energy repository for defense-related transuranic waste. It is located in southeast New Mexico at a depth of 655 m in the Salado Formation, a Permian bedded-salt formation. Cellulosic, plastic, and rubber materials are included in the waste containers as actinide-contaminated waste. This includes lab coats, plastic bottles, rubber gloves, as well as waste-emplacement materials such as wood palettes, plastic wrap, and slip sheets. Possible microbial degradation of cellulosic, plastic, and rubber materials could generate carbon dioxide (CO<sub>2</sub>). Carbon dioxide dissolution would acidify the brine, which would directly affect actinide speciation and solubilities. Therefore, MgO is emplaced in the WIPP repository to reduce actinide solubilities by sequestering CO<sub>2</sub>. In addition, after the WIPP is filled and sealed, the periclase in the MgO will react with water in the gas phase or in brine to form brucite (Mg(OH)<sub>2</sub>). The brucite dissolution reaction will increase the pH to about 9 [1]. A series of experiments was conducted at Sandia National Laboratories to

quantify the efficacy of MgO from Martin Marietta Magnesia Specialties LLC. Martin Marietta (MM) MgO WTS-60 is the MgO currently being emplaced in the WIPP. In this paper we will present the experimental results from MgO characterization and accelerated inundated hydration experiments.

The objectives of MgO characterization were to determine the mineralogic composition and particle-size distribution, and to address uncertainties concerning the amount of reactive constituents, periclase (MgO) plus lime (CaO).

Particle size, solid-to-liquid ratio, and stir speed all affect the rate of carbonation of MgO slurries [2]. It is reasonable to hypothesize that these factors will also affect the rate of hydration. The objectives of the accelerated inundated hydration experiments were to gauge the effect of each of the factors above. We then fitted the accelerated inundated hydration data to various reaction models assuming surface or diffusive control of the hydration process.

## EXPERIMENTAL

All experiments discussed herein were conducted using MM MgO WTS-60. The MgO particle-size distribution was determined as a function of mass fraction by passing MM MgO through Fisher Scientific sieves ranging from 75  $\mu\text{m}$  (200 mesh) to 2.0 mm (10 mesh). The fractions between each pair of sieves (or above and below the sieve for the largest and smallest) were then collected and weighed.

Lower bounds on the amounts of Mg, Al, Si, Ca, and Fe were determined by dissolving samples of MM MgO in trace-metal-grade nitric acid followed by analysis using a Perkin Elmer Optima 3300 DV inductively coupled plasma atomic emission spectrometer (ICP-AES). Scanning-electron-microscope (SEM) images and energy dispersive spectra (EDS) were taken of as-received MM MgO, and of the insoluble portion after dissolution in nitric acid.

To determine the reactive content of MM MgO, the material was first hydrated in deionized (DI) water at 90 °C for at least 3 days, the time required for most of the periclase and lime in MgO to convert to brucite and portlandite ( $\text{Ca}(\text{OH})_2$ ). Next, loss-on-ignition (LOI) tests and thermogravimetric analysis (TGA) were performed to quantify the amount of brucite and portlandite in the hydrated MgO, based on the mass of water lost at the decomposition temperatures for  $\text{Mg}(\text{OH})_2$  and  $\text{Ca}(\text{OH})_2$ . By assuming that all of the brucite and portlandite will eventually carbonate, the hydration followed by LOI testing allowed us to estimate the amount of MM MgO that is capable of reacting with  $\text{CO}_2$ .

A fractional-factorial experimental matrix (Table I) was designed for the accelerated inundated hydration experiment to determine the factors that are important to MgO hydration. Wheaton serum bottles (125 mL) or Nalgene high density polyethylene centrifuge tubes (30 mL) containing DI water and MM MgO were placed either in a VWR oven, where they were not agitated, or in a New Brunswick Scientific water-bath shaker set to a shaking speed of 150 rpm. Both the oven and water-bath shaker were set to 70 °C. The two MgO particle sizes with the highest particle-size fraction were used in the accelerated inundated hydration experiments. The larger particle-size range had particles with diameters between 1.0 and 2.0 mm, which accounted for 32 wt % of the as-received MM MgO. The smaller range had particles with diameters  $<75 \mu\text{m}$ , 18 wt % of the MM MgO. Three WIPP-relevant MgO-to-liquid ratios, 1 g/mL, 0.4 g/mL, 0.05 g/mL were used in the accelerated inundated hydration experiments. Nemer [3] showed that a range of  $10^{-3}$  to  $10^1$  g/mL brackets the expected range of MgO-to-liquid ratios in the WIPP. Experiments were performed on MM MgO in DI water at 70 °C for 43 days. Duplicate samples

were prepared for each experiment. The solid portion of each hydrated sample was filtered using Whatman #40 filter paper and then dried in lab air. A LOI test was then performed on the dried sample, from which the brucite concentration was calculated.

**Table I.** Accelerated Inundated Hydration Experimental Matrix.

	<b>ID</b>	<b>Motion<sup>1</sup></b>	<b>Particle Size<sup>2</sup></b>	<b>MgO/water Ratio<sup>3</sup></b>
1	Ahy-m-sml-tu	1	1	1
2	Ahy-m(8gmgo)-sml-tu	1	1	2
3	Ahy-m-sml-bo	1	1	3
4	Ahy-m-big-tu	1	2	1
5	Ahy-m(8gmgo)-big-tu	1	2	2
6	Ahy-m-big-bo	1	2	3
7	Ahy-s-sml-tu	2	1	1
8	Ahy-s(8gmgo)-sml-tu	2	1	2
9	Ahy-s-sml-bo	2	1	3
10	Ahy-s-big-tu	2	2	1
11	Ahy-s(8gmgo)-big-tu	2	2	2
12	Ahy-s-big-bo	2	2	3

1. Samples with motion level 1 were placed inside an oven, where they were not agitated. Samples with motion level 2 were shaken at 150 rpm in a water-bath shaker.
2. Particle-size level 1 represents MgO with diameters from 1.0-2.0 mm. Particle-size level 2 has diameters <75  $\mu$ m.
3. Samples with MgO/water ratio level 1 contained 10 g of MM MgO and 10 mL of DI water. Samples with MgO/water ratio level 2 contained 8 g of MM MgO and 20 mL of DI water. Samples with MgO/water ratio level 3 contained 5 g of MM MgO and 100 mL of DI water.

## DISCUSSION

### MgO Characterization

The particle-size distribution of one lot of Martin Marietta (MM) MgO WTS-60 was determined by the method described in the experimental section. The resulting particle-size distribution is similar to the manufacturer's analysis sheet that accompanied the tested lot of MM MgO. Lower bounds on the amounts of Mg, Al, Si, Ca and Fe were determined by ICP-AES as discussed in the experimental section. The results are listed in Table II. Table II represents lower bounds because a small fraction of nitric-acid insolubles remained after dissolution and were not quantitatively analyzed. The insolubles remaining after dissolution amounted to about 0.7 wt % of the MM MgO. SEM and EDS spectra of the insolubles indicated the solids were (1) spinel ( $MgAl_2O_4$ ) or a solid solution of several spinels, such as ( $FeCr_2O_4$ ), hercynite ( $FeAl_2O_4$ ), magnesiochromite ( $MgCr_2O_4$ ); (2)  $Fe_2O_3$ ; and (3)  $SiO_2$  (polymorph yet to be determined).

**Table II.** Weight percent of Mg, Al, Si, Ca and Fe (reported as oxides) that dissolved in nitric acid. MgO, Al<sub>2</sub>O<sub>3</sub>, SiO<sub>2</sub>, CaO and Fe<sub>2</sub>O<sub>3</sub> are reported here as oxides, which aren't necessarily representative of the actual phases in the MM MgO.

	<b>MgO</b> (wt %)	<b>CaO</b> (wt %)	<b>Al<sub>2</sub>O<sub>3</sub></b> (wt %)	<b>Fe<sub>2</sub>O<sub>3</sub></b> (wt %)	<b>SiO<sub>2</sub></b> (wt %)
Average	98.46	0.87	0.13	0.12	0.31
Standard Deviation (1 $\sigma$ )	2.54	0.03	0.018	0.01	0.01

The concentration of reactive constituents (periclase and lime) in MM MgO was determined as described in the experimental section. The results are shown in Table III. Detailed calculations can be found in reference [4]. The concentration of periclase and lime in MM MgO,  $96 \pm 2$  (1 $\sigma$ ) wt %, is higher than that of Premier MgO, 92 wt % [5]. In addition, we have tested 21 lots of MM MgO supplied to WIPP. In these 21 lots, the average concentration of periclase plus lime is  $98 \pm 0.5$  (1 $\sigma$ ) wt %.

**Table III.** Weight fraction of periclase and lime in (unhydrated) MM MgO.

	<b>Average</b> (wt %)	<b>Standard Deviation</b> (wt %)	<b>Reported Value</b> mean $\pm \sigma$
periclase	94.8	1.72	$95 \pm 2$
lime	0.874	0.0256	$0.87 \pm 0.03$
periclase + lime	95.7	1.74	$96 \pm 2$

### Accelerated Inundated Hydration Experiments

Inundated hydration experiments were performed on MM MgO in DI water at 70 °C for 43 days. The hydration products were examined using X-ray diffraction (XRD) analysis. The XRD patterns showed that brucite was the only hydration product. Portlandite may have formed but the amount was below the XRD detection limit. After 43 days, the large MgO particles were completely converted to brucite, while a small amount of periclase remained in the small MgO particles. Given more time, we expect that the small MgO particles would completely hydrate.

We used the fraction of periclase converted to brucite,  $W$ , as the measure of reaction progress.

$$W = \frac{X_{\text{brucite}}(t)}{X_{\text{periclase}}}, \quad (1)$$

Here  $X_{\text{brucite}}(t)$  is the mole fraction of brucite in the hydrated sample at time  $t$ , and  $X_{\text{periclase}}$  is the initial mole fraction of periclase. MM MgO contains minerals other than periclase and lime. These include spinels and iron oxides as discussed in the MgO characterization section. During this experiment, those unreactive components may not have hydrated. Therefore, the average hydration of the large MgO particles at 43 days was used as a measure of complete hydration

$X_{brucite}(\infty) = X_{periclase}$ . At the end of 43 days, the average W of the small MgO particles was  $W = 0.9735$  and by our above definition the large particles reached  $W=1$ .

Figure 1 shows the reaction progress versus time for the different factors and levels listed in Table I. Figure 1 shows that the small MgO particles hydrated faster than the large MgO particle during the first few days, which is probably due to the larger specific surface area ( $m^2/g$ ) of the small particles. However for the remainder of the experiment, the large-MgO particles hydrated faster than the small particles. There are no obvious differences between the results of the stirred and unstirred experiments. The MgO/water ratio did not significantly influence the hydration rate until later stages of hydration. A Minitab analysis of variance (ANOVA) was performed on the reaction progress (W) as a function of the effect variables (motion, particle size, and MgO/water ratio) at each point in time by multiple linear regression. The Minitab linear regression model confirmed our visual conclusions from Figure 1.

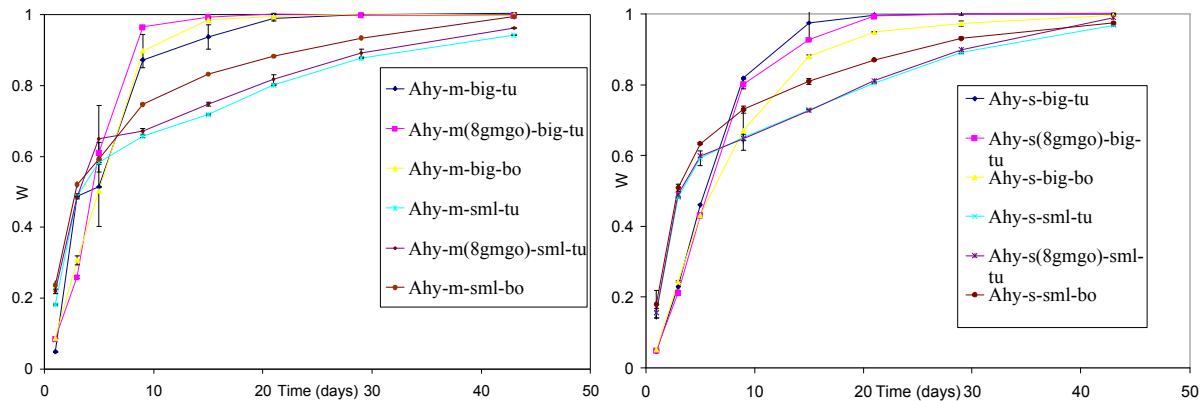


**Figure 1.** MM-MgO hydration progress (W) versus time (days) for experiments carried out in DI water at 70 °C. The results in the left graph are from the unstirred experiments; those on the right were shaken at 150 rpm. The conditions for each sample identified in the legend can be found in Table I.

In dilute solutions, researchers have found that MgO hydration proceeds by the dissolution of MgO followed by precipitation of brucite crystals, usually attached to the MgO surface [6]. Rocha [7] concluded that at high temperature ( $\geq 70$  °C), the hydration of MgO is at first governed by MgO dissolution (surface-area control), then as the reaction progresses both the surface and pores of MgO are covered by  $Mg(OH)_2$ , changing the porosity of the solid. As a result, transport becomes hindered inside particles (diffusive control). Rocha observed that the kinetics of MgO hydration change from surface-area control to diffusive control at  $W > 0.6$ . We fitted the W versus time data to both surface area and diffusion-controlled kinetic models to determine if a particular model or class of models fit the data better than another. The surface-area controlled models assume that the hydration kinetics are controlled by the number of active sites on the reacting surface of a sphere that is shrinking as the reaction proceeds [8]. The diffusion-controlled models assume the kinetics are controlled by diffusion through the brucite layer to the periclase reaction interface [9-10]. Our study shows that different mechanisms may be important for different particle sizes, surface-control for larger particles and diffusion for small particles.

## CONCLUSIONS

MgO characterization and accelerated inundated MgO hydration have been reported in this study. Characterization has shown that the concentration of reactive components (periclase plus lime) in MM MgO is  $96 \pm 2$  wt %. The calculation included conservative assumptions, which decreased the result.

The accelerated inundated hydration experiments were performed to gauge the effects of various factors that could affect the hydration rate, including particle size, solid-to-liquid ratio, and stir speed. As a result of this study we have determined that particle size is the most important factor. In addition, we found that different mechanisms may be important for different particle sizes, surface control for larger particles and diffusion for small particles.

## ACKNOWLEDGMENTS

Sandia is a multi-program laboratory operated by Sandia Corporation, a Lockheed Martin Company, for the United States Department of Energy's National Nuclear Security Administration under Contract DE-AC04-94AL85000. This research is funded by WIPP programs administered by the Office of Environmental Management of the U.S Department of Energy.

## REFERENCES

1. U.S. DOE, *Title 40 CFR Part 191 Compliance Recertification Application for the Waste Isolation Pilot Plant, Appendix BARRIERS* (DOE/WIPP 2004-3231, U.S. Department of Energy Carlsbad Area Office, Carlsbad, NM, (2004).
2. A.I. Fernandez, J.M. Chimenos, M. Segarra, M.A. Fernandez and F. Espiell, *Hydrometallurgy*. **53**, 155-167 (1999).
3. M.B. Nemer, Memo to the records center, ERMS 542612, Sandia National Laboratories, Carlsbad, NM, 2006.
4. H. Deng, Y. Xiong, and M.B. Nemer, Report, ERMS 546570, Sandia National Laboratories, Carlsbad, NM, 2007.
5. A.C. Snider, and Y. Xiong, Analysis report, ERMS 537188, Sandia National Laboratories, Carlsbad, NM, 2004.
6. O. Fruhwirth, G.W. Herzog, I. Hollerer and A. Rachetti, *Surf. Technol.* **24**, 293-300 (1985).
7. S.D. Rocha, M.B. Mansur and V.S. Ciminelli, *J. Chem. Technol. Biotechnol.* **79**, 816-821 (2004).
8. G.K. Layden, and G. W. Brindley, *J. Am. Ceram. Soc.* **46**, 518-522 (1963).
9. R.J. Raymond and G.W. Brindley, *Trans. Faraday Soc.* **61**, 1017-1025 (1964).
10. R.E. Carter, *J. Chem. Phys.* **34**, 2010-2015 (1961)..